

Geo6D: Geometric Constraints Learning for 6D Pose Estimation

Jianqiu Chen^{1*} Mingshan Sun^{2*} Ye Zheng³ Tianpeng Bao² Zhenyu He^{1†}
 Donghai Li² Guoqiang Jin² Rui Zhao² Liwei Wu² Xiaoke Jiang⁴
 Harbin Institute of Technology, Shenzhen¹
 SenseTime Research²
 JD.com, Inc³
 International Digital Economy Academy (IDEA)⁴

Abstract

Existing direct 6D pose estimation methods regress target 6D poses without the need for post-processing, making them effective and easy to develop. However, due to the lack of geometric constraints, the precision of these approaches remains limited, and more training data are required to achieve better performance. To this end, we propose a geometric constraint-based 6D pose estimation method (Geo6D), which establishes an explicit geometric constraint between the input and the regression target. Specifically, a Geo head is proposed to build a point-to-point relationship between the camera frame and the object frame. And additional inputs are introduced as supplementary information to facilitate the learning of the geometric correlation. The proposed Geo6D can be used as a plugin in mainstream direct 6D pose estimation methods. Extensive experimental results show that when equipped with Geo6D, the direct 6D method achieves state-of-the-art performance on multiple datasets and shows significant effectiveness with limited data volume.

1. Introduction

6D pose estimation has drawn widespread attention as the essential prerequisite of emerging applications, such as robotic manipulation, autonomous driving, and augmented reality [5, 26, 3]. Due to the reasonably priced RGB-D sensor, it has become a common practice to estimate 6D pose from RGB-D data, which has been significantly advanced in recent years with deep learning technologies, whether through direct or indirect regression methods. Indirect methods [20, 8, 7] usually first predict an intermediate feature and then use post-processing optimization algorithms, such as least-squares fitting and iterative Perspective-n-

*These authors contributed equally to this work.

†Corresponding authors.

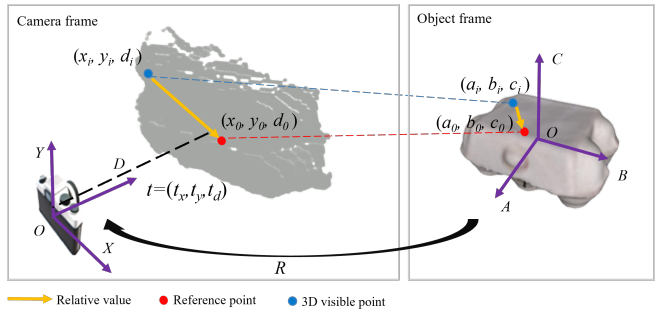


Figure 1: The proposed geometric constraint-based 6D pose estimation. Reformulate the geometric correlation between the camera and object frame within a relative offset representation.

Point (PnP) algorithms [18, 6, 14, 12, 17], to calculate the target pose based on the transformation or projection equation. This approach converts the pose estimation task into two separate stages, allowing the network to fully exploit the geometric constraints of rigid objects to optimize the network in the first stage. However, network optimization in only the first stage is suboptimal, and the second stage’s iterative offline fitting is time-consuming.

Whereas the direct methods [11, 13, 21, 23, 19, 15] predict the final 6D pose directly without post-processing, *i.e.*, which means that the process is efficient and end-to-end. However, since the lack of explicit geometric constraints, the direct regression network requires a large amount of training data to optimize the network fitting the hidden correlation between input data and the output pose parameters. Unfortunately, the data collection and annotation in 6D pose estimation is expensive and synthetic data will inevitably introduce a domain gap problem between training and test dataset. These inevitably severely restrict the model’s performance in practice. Many direct methods[22, 24] introduce the auxiliary loss to regress intermediate geometric

features such as 2D-3D correspondences similar to the indirect method. However, the correlation between pose parameters and input data still is not explicitly established.

Revisiting the transformation equation in Eq. (1), we can observe that the pose parameters (\mathbf{R}, t) and coordinates in the object system (a, b, c) are both unknown to the network. Thus, the model can hardly fit the pose transformation correlation based on this geometric constraint from the input (x, y, d) , rendering pose regression will be an ill-conditioned problem.

$$\begin{bmatrix} x \\ y \\ d \end{bmatrix} = \mathbf{R} \times \begin{bmatrix} a \\ b \\ c \end{bmatrix} + t \quad (1)$$

Moreover, both the object centroid in the camera frame t and visible point coordinates (x, y, d) suffer from a diverse distribution between the training and testing datasets [15]. To address the distribution issue, a vanilla normalization adopted in [15, 4] transforms the coordinates into an offset vector between the visible point (x_i, y_i, d_i) with the 3D mean value of object visible points (x_0, y_0, d_0) , which hold a similar distribution between training and test samples. However, as shown in Eq. (2) the two-point subtract offset representation removes the translation t part. The regression network can hardly learn and optimize the translation part from this equation based on the vanilla normalized coordinates.

$$\begin{bmatrix} x_i - x_0 \\ y_i - y_0 \\ d_i - d_0 \end{bmatrix} = \mathbf{R} \times \begin{bmatrix} a_i - a_0 \\ b_i - b_0 \\ c_i - c_0 \end{bmatrix} + (t - t) \quad (2)$$

To establish an explicit geometric constraint, we propose a geometric constraint-based 6D pose estimation method that enables direct pose regression networks to converge rapidly and reduce the reliance on large amounts of training data. Specifically, we reformulate the transformation equation Eq. (1) into a relative representation by introducing a reference point in both the camera and object frame and divide both sides of the Eq. (1) by the depth value, as shown in Eq. (5). This approach effectively alleviates the distribution gap and retains the translation t part for optimization. For establishing the geometric constraint on the relative offset, we introduce an additional regression head named Geo head to predict the corresponding relative offset value in the object frame. To further facilitate network fitting of the transformation equation, we supplement the additional inputs' feature with $\frac{t_0}{D \cdot d_0}$ and $D \cdot d_0$, which reduces the number of unknown variables and makes the fitted equation more linear.

By explicitly establishing the correlation between pose parameters and input data, our Geo6D accelerates model convergence and reduces data dependencies. It only requires 10% of training data to reach the comparable per-

formance of full training data. Furthermore, we analyze the impact of the Geo6D mechanism from the perspective of the loss function.

To summarize, our main contributions are:

- Propose a geometric constraint-based 6D pose estimation method that establishes an explicit geometric constraint between the input and the regression target for direct methods.
- Introduce additional inputs to linearize and simplify the optimization function
- Extensive experimental results show that the proposed Geo6D can effectively improve the performance and convergence of existing direct regression methods, and achieves state-of-the-art overall results.

2. Related work

We review the indirect and direct 6D pose estimation methods and the current geometric constraints in this section.

2.1. Indirect methods

Indirect methods first predict intermediate geometric information, and then exploit the projection constraints to estimate the 6D pose by optimization function. Recent methods [16, 8, 7] introduce the keypoints mechanism in 6D pose estimation and then estimate the 6D pose by a least-squares fitting algorithm, which takes advantage of the geometric constraints of rigid objects to train the keypoint prediction network. Different from the keypoints-based methods, 2D-3D correspondence-based methods [18, 10, 6, 14, 12, 17] first establish the correspondence between 2D coordinates in the image plane and 3D coordinates in the object coordinate system by the neural network and then solve the 6D pose by a PnP or RANSAC algorithm. However, these indirect methods are only optimized in the first stage rather than the final pose regression, which is suboptimal compared with direct methods. Moreover, the optimization is time-consuming and heavy in practical applications.

2.2. Direct methods

To estimate 6D pose efficiently, recent approaches [15, 11, 13, 21, 23] directly regress the final 6D pose parameters instead of intermediate results. Densefusion [20] extracts geometric and appearance information from RGB-D images individually and fuses them with a dense fusion network. Yet, it ignores the object's 3D coordinates restrictions. Uni6D series [11, 19] simplify the architecture by a single backbone. Uni6D [11] exposes the projection breakdown problem of processing depth images in the CNN framework and first leverages a single homogeneous backbone to process RGB-D data, introducing the extra UV data

into input to preserve the projection constraint. In the following work uni6Dv2 [19], a two-step denoising approach is proposed to guide the network to learn the object-relevant feature and calibrate depth information. However, it is challenging to directly regress the absolute translation without some geometric restrictions and requires more training data. To alleviate the aforementioned problem, ES6D [15] densely regresses offsets from visible points to the centroid point in 3D space. However, The translation part was eliminated in the calculation of the offset, making it an ill-conditioned problem and affecting the convergence of the regression network.

2.3. Geometric constraints in 6D pose estimation

The indirect methods usually utilize different geometric constraints to train a neural network to predict intermediate features such as predefined keypoints and 2D-3D correspondence. It has an explicit correlation between the input and output target features, which is easier for network optimization. Unlike the indirect method, the direct method needs to regress the pose parameters by the network, which restricts the network output target. To provide more geometric constraints information, some methods [22, 24] apply an additional network output head and auxiliary loss to regress intermediate geometric features such as 2D-3D correspondences matrix or render alignment. However, the geometric correlation between the network output pose parameters and input data still are not explicitly established. Hence, we propose the Geo6D mechanism reformulating the input and output to hold the geometric constraint in the relative offset representation and supplement additional geometric values into input to make it easy to be fitted by the network.

3. Method

In this section, we first give an overview of our geometric constraint-based 6D pose estimation method. Then we present the specific adjustments made to the input features and regression targets, and finally, we analyze the impact of the Geo6D mechanism from the perspective of the loss function that balance of rotation and translation part training losses.

3.1. Overview

We summarize our geometric constraint-based 6D pose estimation method in Fig. 2. Given an RGB-D input image, we first take an object instance segmentation model to predict the bounding box and mask of the target object and obtain the patch with absolute XYD data in the camera coordinate system, which is cropped and masked by the results of the instance segmentation network. We then select a reference point inside the object and apply the proposed relative

represented geometric constraint on the patch to get relative offset ΔXYD and ΔABC within the camera and object coordinate frame between visible points and the reference point as defined in Eq. (5). Lastly, feeding the relative input into a 6D pose estimator to get the rotation and relative translation $\Delta \mathbf{t}$, which can be thought of as regression from a reference point (x_0, y_0, d_0) named \mathbf{t}_0 to target translation \mathbf{t} . The final translation result is the summary of the predicted relative one and \mathbf{t}_0 . Besides, the network introduces an extra Geo head to predict the corresponding relative offset value in the object frame ΔABC for the training phase to optimize the network fitting the geometric constraints. For better network convergence, we supplement the input feature with the constraint required variables $D \cdot d_0$ and $\frac{t_0}{D \cdot d_0}$. Following the proposed Geo6D approach, the pose estimation network input and output data could be formulated as:

$$\mathbf{R}, \Delta \mathbf{t}, \Delta ABC = f(\text{RGB}, \Delta XYD, D \cdot d_0, \frac{\mathbf{t}_0}{D \cdot d_0}). \quad (3)$$

3.2. Geometric constraint-based 6D pose estimation

Each visible point (x_i, y_i, d_i) in the camera frame has its corresponding coordinates (a_i, b_i, c_i) in the object frame, which can be calculated by the projection equation according to Eq. (1). Similarly, the mean values of these visible points also satisfy the equation, selecting and denoting this mean value point as the reference point. Then, we calculate the reference point coordinate (x_0, y_0, d_0) or named it \mathbf{t}_0 and (a_0, b_0, c_0) in both the camera and object frame. We simultaneously divide both sides of the equation by the depth value d , as shown in Eq. (4) to avoid the optimization issue within the vanilla normalization.

$$\begin{bmatrix} \frac{x_i}{d_i} \\ \frac{y_i}{d_i} \\ \frac{c_i}{d_i} \\ 1 \end{bmatrix} = \mathbf{R} \times \begin{bmatrix} \frac{a_i}{d_i} \\ \frac{b_i}{d_i} \\ \frac{c_i}{d_i} \\ \frac{d_i}{d_i} \end{bmatrix} + \frac{\mathbf{t}}{d_i} \quad (4)$$

According to Eq. (4), both sides of the equation subtract the reference point coordinates divided by d_0 in the camera frame $(\frac{x_0}{d_0}, \frac{y_0}{d_0}, 1)$ and the object frame $(\frac{a_0}{d_0}, \frac{b_0}{d_0}, \frac{c_0}{d_0})$ respectively. The transformation constraint about a visible point and the reference point is reformulated in relative value holding the geometric constraint in relative offset representation.

$$\begin{bmatrix} \Delta x \\ \Delta y \\ 0 \end{bmatrix} = \mathbf{R} \times \begin{bmatrix} \frac{a_i}{d_i} - \frac{a_0}{d_0} \\ \frac{b_i}{d_i} - \frac{b_0}{d_0} \\ \frac{c_i}{d_i} - \frac{c_0}{d_0} \\ \frac{d_i}{d_i} - \frac{d_0}{d_0} \end{bmatrix} - \frac{\Delta d}{d_i d_0} \Delta \mathbf{t} - \frac{\mathbf{t}_0}{d_i d_0} \quad (5)$$

where

$$\Delta x = \frac{x_i}{d_i} - \frac{x_0}{d_0}, \Delta y = \frac{y_i}{d_i} - \frac{y_0}{d_0}$$

$$\Delta d = d_i - d_0, \Delta \mathbf{t} = \mathbf{t} - \mathbf{t}_0$$

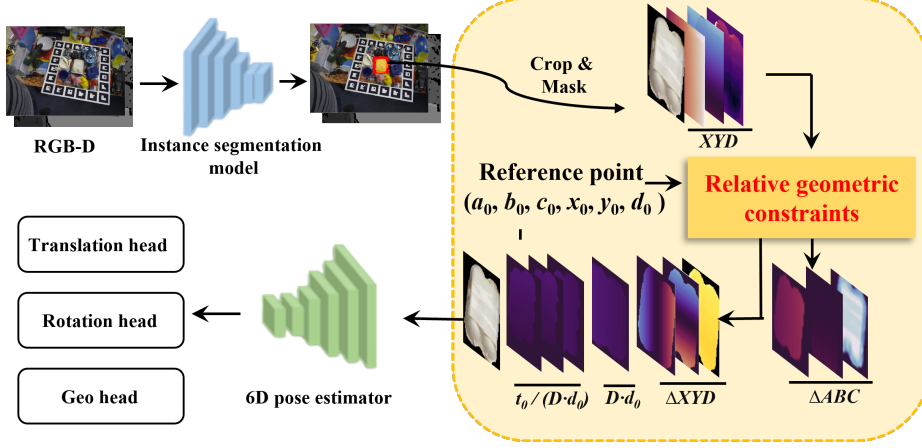


Figure 2: Overview of our proposed Geo6D pose estimation process. Reformulate input data based on the relative offset geometric constraint and introduce a Geo head to regress ΔABC . The final translation t is calculated by adding the reference point coordinate t_0 with predicted offsets Δt .

$$\Delta ABC = \begin{bmatrix} \frac{a_i}{d_i} - \frac{a_0}{d_0} \\ \frac{b_i}{d_i} - \frac{b_0}{d_0} \\ \frac{c_i}{d_i} - \frac{c_0}{d_0} \end{bmatrix}.$$

To establish an explicit geometric constraint, we adopt the ΔABC serving as an additional regression target of Geo head to optimize and learn the transformation equation. Taking into account the missing variables $d_i d_0$ and $\frac{t_0}{d_i d_0}$ in the input data, we introduced them as additional inputs to linearize and simplify the optimization function, making it easier to fit the network. Further comparisons of our geometric constraint-based mechanism design are presented in our ablation study.

3.3. Balanced ADD loss

To train the network to estimate 6D pose, ADD loss is a common choice for most methods. It heterogeneously transforms the points sampled on the object CAD model by the predicted poses and ground truth. It minimizes the distances of corresponding points between two different transformation points set. The specific loss is defined as

$$L_{ADD} = \frac{1}{m} \sum_j \|(\mathbf{R}x_j + \mathbf{t}) - (\hat{\mathbf{R}}x_j + \hat{\mathbf{t}})\|_2^2 \quad (6)$$

where x_j is the j^{th} point from m randomly sampled CAD model's 3D points in the object frame, (\mathbf{R}, \mathbf{t}) is the predicted pose and $(\hat{\mathbf{R}}, \hat{\mathbf{t}})$ is the ground truth pose. Recombin-

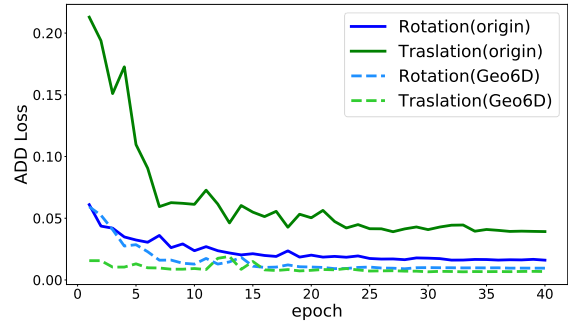


Figure 3: Balanced ADD loss on the Occlusion LineMOD dataset.

ing Eq. (6), it can be reformulated as:

$$\begin{aligned} L_{ADD} &= \frac{1}{m} \sum_j \|(\Delta \mathbf{R}x_j + \Delta \mathbf{t})\|_2^2 \\ &= \frac{1}{m} \sum_j (\|\Delta \mathbf{R}x_j\|_2^2 + 2\Delta \mathbf{R}x_j \Delta \mathbf{t} + \|\Delta \mathbf{t}\|_2^2) \\ &= \frac{1}{m} \sum_j (\|\Delta \mathbf{R}x_j\|_2^2) + 2\Delta \mathbf{R} \sum_j x_j \Delta \mathbf{t} + \|\Delta \mathbf{t}\|_2^2 \end{aligned} \quad (7)$$

where

$$\Delta \mathbf{R} = \mathbf{R} - \hat{\mathbf{R}}$$

$$\Delta \mathbf{t} = \mathbf{t} - \hat{\mathbf{t}}.$$

Since x_j is sampled from the object frame, the centroid of sampled points is approx to the origin that $\sum_j x_j \approx 0$.

Hence, the ADD loss is approximately equal to

$$L_{ADD} \approx \frac{1}{m} \sum_j (\|\Delta \mathbf{R}x_j\|_2^2) + \|\Delta \mathbf{t}\|_2^2 \quad (8)$$

which consists of the rotation part $\frac{1}{m} \sum_j (\|\Delta \mathbf{R}x_j\|_2^2)$ and translation part $\|\Delta \mathbf{t}\|_2^2$. For the rotation part, since any point on the object after rotating is inside the object’s circumscribed sphere, the rotation part is bounded by the object’s diameter. However, the translation part is unbounded because \mathbf{t} and $\hat{\mathbf{t}}$ are absolute 3D translate vectors, denoting the centroid of the object in the camera frame, which can be any position in the 3D space. Hence, when $\|\Delta \mathbf{t}\|_2^2 \gg 2 * r$, the translation part may dominate the optimization, and the rotation part will be neglected. The loss will be degraded to the l_2 loss to fit the absolute value of the translation vector. As shown in Fig. 3, the ADD loss has an obvious imbalance between the rotation and translation part, where the translation part occupies the majority.

After adopting the Geo6D, the regression target translation vector is instead by an equivalent offset value between the object centroid and the reference point, which range is transformed into the range $(-r, r)$ comparable to the rotation part. Therefore, the rotation and translation parts are balanced in the same magnitude. Hence, the rotation part is able to converge faster and the balanced loss shows better optimization results. The balanced ADD loss optimizes the regression network to find correspondences between input data and the CAD model transformed by rotation and the offset translate vector. Hence, the Geo6D mechanism fixes the ADD loss degradation and simplifies the pose estimation task.

4. Experiments

4.1. Benchmark datasets

We conduct our experiments on four benchmark datasets.

LineMOD [9] contains 13 sequences of 13 low-textured objects. Since there is only about 1.2k real training data annotated with 6D pose, we follow previous work [16, 25, 8, 11] to add synthetic images for training with 99.71% synthetic ratio.

Occlusion LineMOD [1] consists of 1214 testing images that are selected from the LineMOD dataset in the occlusion scene. Since there is no extra real training data, the training dataset is the same as LineMOD. The domain gap between training and testing datasets, as well as the heavily occluded objects, make it more challenging for 6D pose estimation.

YCB-Video [2] is a large and challenging dataset that contains 21 objects with 92 RGB-D sequences. It provides a large amount of real training data holding the same pose distribution between training and testing datasets.

It exists significant location distribution and style gaps between training and testing datasets, which is challenging for methods to handle these domain gaps.

4.2. Evaluation metrics

We adopt the commonly used average distance metrics ADD, ADD-S, and ADD(S) to evaluate different methods. ADD evaluates the mean of pairwise distance between two object point clouds which are transformed according to the ground truth pose $[\mathbf{R}, \mathbf{t}]$ and the predicted pose $[\hat{\mathbf{R}}, \hat{\mathbf{t}}]$ respectively:

$$ADD = \frac{1}{m} \sum_{x \in \mathcal{O}} \|(\mathbf{R}x + \mathbf{t}) - (\hat{\mathbf{R}}x + \hat{\mathbf{t}})\| \quad (9)$$

where \mathcal{O} denotes the 3D model of an object, x denotes any point on the model and m denotes total point number in the model. To alleviate the ambiguous matching of the symmetric objects, ADD-S is adopted to estimate the closest point distance between two point clouds:

$$ADD-S = \frac{1}{m} \sum_{x_1 \in \mathcal{O}} \min_{x_2 \in \mathcal{O}} \|(\mathbf{R}x_1 + \mathbf{t}) - (\hat{\mathbf{R}}x_2 + \hat{\mathbf{t}})\|. \quad (10)$$

For convenience, we introduce ADD(S) metric:

$$ADD(S) = \begin{cases} ADD & \mathcal{O} \text{ is asymmetric} \\ ADD-S & \mathcal{O} \text{ is symmetric} \end{cases} \quad (11)$$

For LineMOD and Occlusion LineMOD datasets, we choose the threshold with 0.1d (10% of the diameter of the object) to calculate the accuracy of ADD(S), following [16, 7]. For the YCB-Video dataset, following [25, 20, 8, 7, 15], we calculate the AUC (area under the accuracy-threshold curve) of ADD(S) with a maximum threshold of 0.1 meters.

4.3. Apply Geo6D to different methods

To verify the extensibility of the proposed Geo6D, we apply it to ES6D [15] and Uni6Dv2 [19]. These two methods have different frameworks, output formats, and loss functions.

Apply Geo6D mechanism to Uni6Dv2. The input of Uni6Dv2 consists of an image patch (RGB, X, Y, D, NRM) which is cropped by the prediction of the segmentation network in the first stage. Then, the sparse regression network based on the image patch regresses the rotation and 3D location in the camera frame for each object and trains it through ADD Loss. To apply the Geo6D mechanism to Uni6Dv2, we replace the visible points’ absolute positional encoding part (X, Y, D) with relative values $(\Delta X, \Delta Y, \Delta D)$ between visible points to the reference point and following the Eq. (5) supplements

	Geo6D	Occlusion LineMOD	LineMOD	YCB-Video
Uni6Dv2	w/o	40.6	97.2	91.5
Uni6Dv2	w	79.8(+39.2)	99.6(+2.4)	91.6(+0.1)

Table 1: Evaluation results of Uni6Dv2 with Geo6D on Occlusion LineMOD, LineMOD and YCB-Video datasets.

Setting	Geo6D	10% R+10%S	10% R+100%S	100% R+100%S
ES6D	w/o	83.6	90.1	93.2
ES6D	w	84.7(+1.1)	92.3(+2.2)	93.6(+0.4)
Uni6Dv2	w/o	79.7	88.0	91.5
Uni6Dv2	w	86.5(+6.8)	89.3(+1.3)	91.6(+0.1)

Table 2: Evaluation results of ES6D and Uni6Dv2 with Geo6D on YCB-Video dataset with different amounts of training data. R means real data and S means synthetic data.

the additional component concatenating with input data among channel.

For the output part, we apply an additional Geo head to regress visible points’ ΔABC and adjust the regression target of the original translation head reformulated as the offset of the reference point to the centroid Δt . The comparison results are shown in Tab. 1. After adopting the Geo6D mechanism to Uni6Dv2, it shows an obvious improvement(+39.2%) on the Occlusion LineMOD. Due to the advance of network convergence, adopting Geo6D shows significantly greater improvements in fewer amounts of training data demonstrated in Tab. 2.

Apply Geo6D mechanism to ES6D. The original ES6D feeds cropped RGB images with vanilla normalized (x, y, d) and leverages a dense regression network to predict the offsets of visible points to the centroid of an object and a confidence score. It introduces an A(M)GPD loss to replace the ADD loss to train the network. The final pose is selected by the point with the highest confidence score. To apply the Geo6D mechanism to ES6D, the input is changed as the Eq. (5). Introduce an additional Geo head with the same structure as the translation head to regress ΔABC . Since ES6D does not provide the Occlusion LineMOD result, we implement it on the YCB-Video dataset and since its limitation of sensitivity to mask results, all results are based on Ground Truth segmentation masks. We provide the results about the different amounts of training data in Tab. 2. Geo6D mechanism leverages explicit geometric constraints and solves the translate part optimization issue in vanilla normalization. Experiments on Tab. 2 show significantly further improvements in fewer amounts of training data, demonstrating their effectiveness on the dense regression method.

class	PoseCNN	PVN3D	FFB6D	Uni6D	Uni6Dv2	Ours
ape	9.6	33.9	47.2	33.0	44.3	64.6
can	45.2	88.6	85.2	51.1	53.3	91.5
cat	0.9	39.1	45.7	4.6	16.7	63.2
driller	41.4	78.4	81.4	58.4	63.0	82.3
duck	19.6	41.9	53.9	34.8	51.6	63.9
eggbox	22.0	80.9	70.2	1.7	4.6	95.4
glue	38.5	68.1	60.1	30.2	40.3	95.0
holepuncher	22.1	74.7	85.9	32.1	50.9	82.6
Avg	24.9	63.2	66.2	30.7	40.6	79.8

Table 3: Evaluation results on the Occlusion LineMOD dataset. Symmetric objects are denoted in bold. "Ours" is Uni6Dv2+Geo6D.

4.4. Comparison with SOTA methods

We provide comprehensive and detailed comparison results on Occlusion LineMOD, LineMOD, and YCB-Video datasets. For the brevity of the paper, category-level experimental results on YCB-Video are provided in Supplementary Materials.

Evaluation on Occlusion LineMOD dataset. The quantitative results on the Occlusion LineMOD dataset are presented in Tab. 3. Compared with the baseline Uni6Dv2, employing the Geo6D mechanism achieves a significant improvement (+39.2%) on ADD(S) metric and outperforms state-of-the-art method FFB6D [7](indirect method) by 13.6%. Noteworthy, adopting the Geo6D mechanism makes the network more reliable when there are significant translation distribution gaps.

Evaluation on LineMOD dataset. The quantitative results on the LineMOD dataset are presented in Tab. 4. Compared with our baseline Uni6Dv2, introducing the Geo6D mechanism brings a 2.5% performance gain on ADD(S), demonstrating the effectiveness of our Geo6D mechanism. Compared to FFB6D [7], the performance gap is minimal (99.6% vs. 99.7%), while our Geo6D-based direct method has a more straightforward design and faster speed.

Evaluation on YCB-Video dataset. The quantitative results on the YCB-Video dataset are presented in Tab. 5. We provide the implementations on the baseline Uni6Dv2 and ES6D, and introducing the Geo6D mechanism brings a 0.1% and 0.4% performance gain on the AUC of ADD(S) for full training data. Due to the large amount of data in the YCBV dataset, the network can be able to fit some variables, resulting in a relatively small improvement with the full dataset. As the result in Tab. 2, the fewer training data, our method can achieve greater improvement.

In summary, our Geo6D mechanism makes direct 6D pose estimation methods outperform indirect methods on Occlusion LineMOD and YCB-Video datasets, and achieve comparable accuracy on the LineMOD dataset.

	PoseCNN	DenseFusion	PVN3D	FFB6D	Uni6D	Uni6Dv2	Ours
ape	77.0	92.3	97.3	98.4	93.7	95.7	98.3
benchvise	97.5	93.2	99.7	100.0	99.8	99.9	100.0
camera	93.5	94.4	99.6	99.9	96.0	95.8	99.6
can	96.5	93.1	99.5	99.8	99.0	96.0	99.9
cat	82.1	96.5	99.8	99.9	98.1	99.2	100.0
driller	95.0	87.0	99.8	100.0	99.1	99.2	99.8
duck	77.7	92.3	97.7	98.4	90.0	92.1	97.4
eggbox	97.1	99.8	99.8	100.0	100.0	100.0	100.0
glue	99.4	100.0	100.0	100.0	99.2	99.6	100.0
holepuncher	52.8	92.1	99.9	99.8	90.2	92.0	99.7
iron	98.3	97.0	99.7	99.9	99.5	98.0	100.0
lamp	97.5	95.3	99.8	99.9	99.4	98.5	99.9
phone	87.7	92.8	99.5	99.7	97.4	97.7	99.8
Avg	88.6	94.3	99.4	99.7	97.0	97.2	99.6

Table 4: Evaluation results on the LineMOD dataset. Symmetric objects are denoted in bold. "Ours" is Uni6Dv2+Geo6D

	PoseCNN	DenseFusion	PVN3D	FFB6D	Uni6D	Uni6Dv2	ES6D	Uni6Dv2+Geo6D	ES6D+Geo6D
Avg	59.9	82.9	91.8	92.7	88.8	91.5	93.2	91.6	93.6

Table 5: Evaluation results on the YCB-Video dataset.

Effect of different components in transformation equation components		setting	ADD(S)
(1): XYD value		absolute value	8.5
		offset value	70.7
(2): (1) + Geo head		absolute value: a_i	70.8
		offset value: $a_i - a_0$	71.1
		offset value: $\frac{a_i}{d_i} - \frac{a_0}{d_0}$	72.8
(3): (2) + $D \cdot d_0$ input		vanilla normalized XYD with $D \cdot d_0$	73.1
		proposed normalized XYD with $D \cdot d_0$	73.7
(4): (3) + $\frac{t_0}{D \cdot d_0}$ input		$\frac{t_0}{D \cdot d_0}$ input	74.2

Table 6: Effect of different components in transformation equation. The best setting in the previous row serves as the benchmark for the next row.

4.5. Ablation study

In this section, we will analyze the effectiveness of the Geo6D mechanism and compare different reference point generation strategies on Uni6Dv2. All experiments are conducted on the Occlusion LineMOD dataset with 10% training data.

Effect of different components in translation equation. To analyze the effect of each input and output components adjustment, an ablation study is conducted by modifying or adding one of the components in the proposed geometric constraint equation Eq. (5). As reported in Tab. 6, the ΔXYD significantly improves by solving the distribution gap issue. Based on the offset representation, introducing

Reference point generation strategies		ADD(S)
x_0 and y_0	d_0	
Projection values	nearest depth point	66.7
Projection values	mean depth point	72.7
mean of visible points	mean of visible points	74.2

Table 7: Comparison of generation strategies for the reference point (x_0, y_0, d_0) . "Projection values" denotes calculating from the pin-hole projection equation

the Geo head shows an advanced performance when choosing the optimization target following the proposed relative offset ΔABC as shown in Eq. (5). Taking a channel as an example, the relative offset format $\frac{a_i}{d_i} - \frac{a_0}{d_0}$ follows the equation and achieves the better performance gain. Compared with only applying the Geo head, additional input of the components $D \cdot d_0$ and $\frac{t_0}{D \cdot d_0}$ can indeed advance the performance. Furthermore, as the result in the (3) row, the proposed relative offset representation $(\frac{x_i}{d_i} - \frac{x_0}{d_0})$ outperforms the vanilla normalization $(x_i - x_0)$, demonstrating the advantage of introducing the translate vector into optimization.

Effect and efficiency of the Geo6D mechanism. We analyze the effect of different relative offset representation strategies, including the vanilla 3D normalization and the proposed relative offset representation. When only introducing the vanilla normalization into UniDv2 to regress a relative offset, the performance of Uni6Dv2 improves by

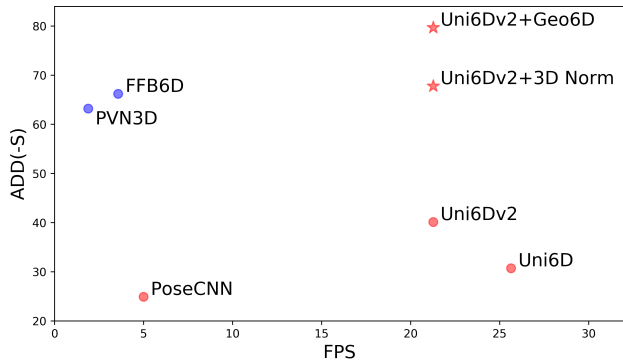


Figure 4: Comparison of speed and accuracy on the Occlusion LineMOD with full amount training data: Uni6Dv2+Geo6D achieves state-of-the-art accuracy in both direct regression methods (red dots) and indirect regression methods (blue dots) methods. 3D norm denotes that only adopts the vanilla normalization.

27.2%, achieving 67.8% w.r.t ACC-ADD(S). When adopting the proposed Geo6D mechanism to Uni6Dv2, there is an obvious performance gain from 40.6% to 79.8%, and it shows a 12% advanced improvement compared with Uni6Dv2 equipped with 3D vanilla normalization. Moreover, for analyzing efficiency, as shown in Fig. 4, the relative offset representation merely does not introduce extra time consumption and helps Uni6Dv2 outperform the current SOTA RGB-D method FFB6D [7] 13.6% while 5.6 times faster than it. The improvement demonstrates that the proposed geometric constraint can facilitate direct network higher performance without sacrificing the efficiency.

Reference point generation strategies. To build a stable reference point, we attempt three different reference point generation strategies, as shown in Tab. 7. The first strategy selects the 2D coordinate UV value (u_0, v_0) of the ROI region center, the nearest point’s depth as reference point depth d_0 , and then calculates x_0 and y_0 based on pin-hole projection equation. The ROI center as the reference point in the 2D image plane maintains a stable UV encoding and attempts to use the center point’s depth to project the reference point in the 3D space. However, since the center point in ROI is likely in the outside or margin of the object due to the occlusion or the irregular, the depth value may be lost or a noise point from the sensor. To alleviate this problem, the second strategy adopts the mean depth value of the object region as the reference depth, which improves the stability of the Geo6D mechanism, achieving a 6% improvement from 66.7% to 72.7%. Besides the reference point selection based on the UV, the third strategy adopts the mean XYD of visible points as the reference point. Compared with the selection from UV, it is prone to

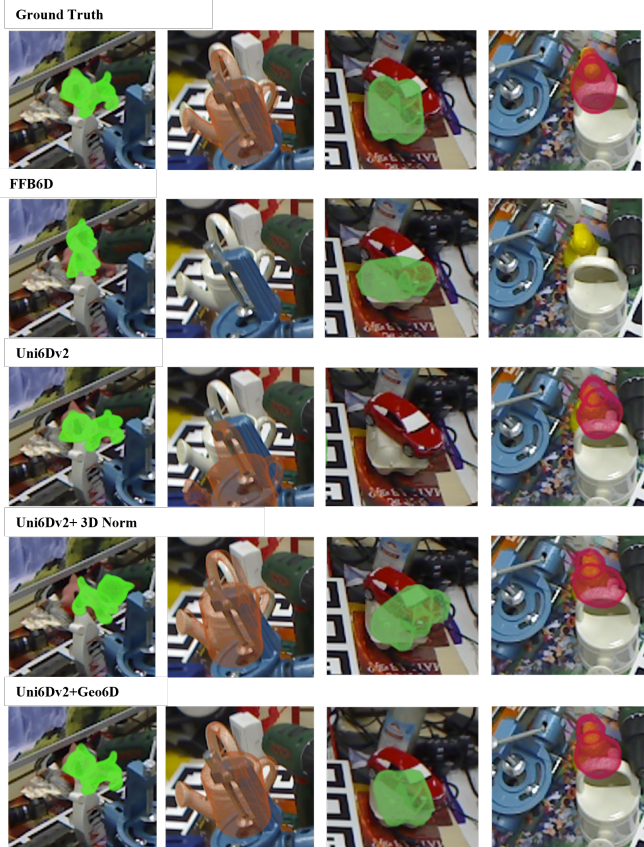


Figure 5: Qualitative results of 6D pose estimation on the Occlusion LineMOD dataset. 3D norm denotes that only adopts the vanilla normalization.

consider the 3D shape and shows better performance than the UV selection strategy. Hence, whatever the reference point generation considers the 2D shape or 3D shape, the Geo6D mechanism can demonstrate its effectiveness.

4.6. Visualization

Visualization results of the Occlusion LineMOD dataset are shown in Fig. 5. We can observe that Uni6Dv2+Geo6D could predict a more precise and robust 6D pose on the heavily occluded objects compared to other methods. Moreover, benefiting from the Geo6D mechanism, the orientation of objects with only a few visible points is correctly predicted, which proves that the proposed Geo6D mechanism improves the robustness and generalization of the network.

5. Conclusion

In this paper, we proposed a novel method named Geo6D which achieves state-of-the-art performance on multiple benchmarks for 6D pose estimation. A non-ill-conditioned 6D pose transformation is derived at first. Based on

the derived transformation, Geo6D utilizes a Geo head to strengthen the point-to-point relationship between the camera frame and the object frame. Moreover, some items in the derived transformation are fed into neural networks as extra information to facilitate the learning of the geometric correlation. Extensive experiments show that Geo6D makes the 6D pose estimation task much easier and can be plugged into different direct methods such as Uni6Dv2 and ES6D. Experiments also prove that Geo6D achieves more gains with limited training data volume. We believe that the Geo6D mechanism is able to inspire other 3D tasks, such as category-level pose estimation, and 3D object detection with RGB-D or Lidar data.

As for limitations, the current reference point generation strategy in Geo6D requires that the mean point is close to most objects' centroid. When the mean point of irregular objects is far away from the centroid, Geo6D is hard to generate a stable reference point on the CAD model. Therefore, more effective generation strategies need to be explored when handling irregular objects.

References

- [1] Eric Brachmann, Alexander Krull, Frank Michel, Stefan Gumhold, Jamie Shotton, and Carsten Rother. Learning 6d object pose estimation using 3d object coordinates. In *European conference on computer vision*, pages 536–551, 2014.
- [2] Berk Calli, Arjun Singh, Aaron Walsman, Siddhartha Srinivasa, Pieter Abbeel, and Aaron M Dollar. The ycb object and model set: Towards common benchmarks for manipulation research. In *2015 international conference on advanced robotics (ICAR)*, pages 510–517, 2015.
- [3] Xiaozhi Chen, Huimin Ma, Ji Wan, Bo Li, and Tian Xia. Multi-view 3d object detection network for autonomous driving. In *Proceedings of the IEEE conference on Computer Vision and Pattern Recognition*, pages 1907–1915, 2017.
- [4] Zheng Dang, Lizhou Wang, Yu Guo, and Mathieu Salzmann. Learning-based point cloud registration for 6d object pose estimation in the real world. In *European Conference on Computer Vision (ECCV) 2022*, October 2022.
- [5] Andreas Geiger, Philip Lenz, and Raquel Urtasun. Are we ready for autonomous driving? the kitti vision benchmark suite. In *2012 IEEE conference on computer vision and pattern recognition*, pages 3354–3361, 2012.
- [6] Rasmus Laurvig Haugaard and Anders Glent Buch. Surfemb: Dense and continuous correspondence distributions for object pose estimation with learnt surface embeddings. In *Proceedings of the IEEE/CVF Conference on Computer Vision and Pattern Recognition*, pages 6749–6758, 2022.
- [7] Yisheng He, Haibin Huang, Haoqiang Fan, Qifeng Chen, and Jian Sun. Ffb6d: A full flow bidirectional fusion network for 6d pose estimation. In *Proceedings of the IEEE/CVF Conference on Computer Vision and Pattern Recognition*, pages 3003–3013, 2021.
- [8] Yisheng He, Wei Sun, Haibin Huang, Jianran Liu, Haoqiang Fan, and Jian Sun. Pvn3d: A deep point-wise 3d keypoints voting network for 6dof pose estimation. In *Proceedings of the IEEE/CVF conference on computer vision and pattern recognition*, pages 11632–11641, 2020.
- [9] Stefan Hinterstoisser, Stefan Holzer, Cedric Cagniart, Slobodan Ilic, Kurt Konolige, Nassir Navab, and Vincent Lepetit. Multimodal templates for real-time detection of texture-less objects in heavily cluttered scenes. In *2011 international conference on computer vision*, pages 858–865, 2011.
- [10] Tomas Hodan, Daniel Barath, and Jiri Matas. Epos: Estimating 6d pose of objects with symmetries. In *Proceedings of the IEEE/CVF conference on computer vision and pattern recognition*, pages 11703–11712, 2020.
- [11] Xiaoke Jiang, Donghai Li, Hao Chen, Ye Zheng, Rui Zhao, and Liwei Wu. Uni6d: A unified cnn framework without projection breakdown for 6d pose estimation. *IEEE/CVF Conference on Computer Vision and Pattern Recognition (CVPR)*, 2022.
- [12] P Kiru, Timothy Patten, and MV Pix2Pose. Pixel-wise coordinate regression of objects for 6d pose estimation. *Proceedings of the ICCV, Seoul, Korea*, pages 27–28, 2019.
- [13] Yi Li, Gu Wang, Xiangyang Ji, Yu Xiang, and Dieter Fox. Deepim: Deep iterative matching for 6d pose estimation. In *Proceedings of the European Conference on Computer Vision (ECCV)*, pages 683–698, 2018.
- [14] Zhigang Li, Gu Wang, and Xiangyang Ji. Cdpn: Coordinates-based disentangled pose network for real-time rgb-based 6-dof object pose estimation. In *Proceedings of the IEEE/CVF International Conference on Computer Vision*, pages 7678–7687, 2019.
- [15] Ningkai Mo, Wanshui Gan, Naoto Yokoya, and Shifeng Chen. Es6d: A computation efficient and symmetry-aware 6d pose regression framework. In *Proceedings of the IEEE/CVF Conference on Computer Vision and Pattern Recognition*, pages 6718–6727, 2022.
- [16] Sida Peng, Yuan Liu, Qixing Huang, Xiaowei Zhou, and Hujun Bao. Pvnnet: Pixel-wise voting network for 6dof pose estimation. In *Proceedings of the IEEE/CVF Conference on Computer Vision and Pattern Recognition*, pages 4561–4570, 2019.
- [17] Mahdi Rad and Vincent Lepetit. Bb8: A scalable, accurate, robust to partial occlusion method for predicting the 3d poses of challenging objects without using depth. In *Proceedings of the IEEE international conference on computer vision*, pages 3828–3836, 2017.
- [18] Yongzhi Su, Mahdi Saleh, Torben Fetzter, Jason Rambach, Nassir Navab, Benjamin Busam, Didier Stricker, and Federico Tombari. Zebrapose: Coarse to fine surface encoding for 6dof object pose estimation. In *Proceedings of the IEEE/CVF Conference on Computer Vision and Pattern Recognition*, pages 6738–6748, 2022.
- [19] Mingshan Sun, Ye Zheng, Tianpeng Bao, Jianqiu Chen, Guoqiang Jin, Rui Zhao, Liwei Wu, and Xiaoke Jiang. Uni6dv2: Noise elimination for 6d pose estimation. *arXiv preprint arXiv:2208.06416*, 2022.
- [20] Chen Wang, Danfei Xu, Yuke Zhu, Roberto Martín-Martín, Cewu Lu, Li Fei-Fei, and Silvio Savarese. Densefusion: 6d object pose estimation by iterative dense fusion. In *Proceed-*

ings of the IEEE/CVF conference on computer vision and pattern recognition, pages 3343–3352, 2019.

- [21] Gu Wang, Fabian Manhardt, Jianzhun Shao, Xiangyang Ji, Nassir Navab, and Federico Tombari. Self6d: Self-supervised monocular 6d object pose estimation. In *European Conference on Computer Vision*, pages 108–125. Springer, 2020.
- [22] Gu Wang, Fabian Manhardt, Jianzhun Shao, Xiangyang Ji, Nassir Navab, and Federico Tombari. Self6d: Self-supervised monocular 6d object pose estimation. In *European Conference on Computer Vision*, pages 108–125, 2020.
- [23] Gu Wang, Fabian Manhardt, Federico Tombari, and Xiangyang Ji. Gdr-net: Geometry-guided direct regression network for monocular 6d object pose estimation. In *Proceedings of the IEEE/CVF Conference on Computer Vision and Pattern Recognition*, pages 16611–16621, 2021.
- [24] Gu Wang, Fabian Manhardt, Federico Tombari, and Xiangyang Ji. Gdr-net: Geometry-guided direct regression network for monocular 6d object pose estimation. In *Proceedings of the IEEE/CVF Conference on Computer Vision and Pattern Recognition*, pages 16611–16621, 2021.
- [25] Yu Xiang, Tanner Schmidt, Venkatraman Narayanan, and Dieter Fox. Posecnn: A convolutional neural network for 6d object pose estimation in cluttered scenes. In *Robotics: Science and Systems (RSS)*, 2018.
- [26] Danfei Xu, Dragomir Anguelov, and Ashesh Jain. Pointfusion: Deep sensor fusion for 3d bounding box estimation. In *Proceedings of the IEEE conference on computer vision and pattern recognition*, pages 244–253, 2018.